Rapid carbon mineralization for permanent disposal of anthropogenic carbon dioxide emissions

Juerg M. Matter[1,2*], Martin Stute[2], Sandra Ó. Snæbjörnsdottir[3], Eric H. Oelkers[3,4,5], Sigurdur R. Gislason[3], Edda S. Aradottir[6], Bergur Sigfusson[6,7], Ingvi Gunnarsson[6], Holmfridur Sigurdardottir[6], Einar Gunnlaugsson[6], Gudni Axelsson[8], Helgi A. Alfredsson[3], Domenik Wolff-Boenisch[3,9], Kiflom Mesfin[3], Diana Fernandez de la Reguera Taya[2], Jennifer Hall[2], Knud Dideriksen[10], Wallace S. Broecker[2]

[1]Ocean and Earth Science, University of Southampton, UK

[2]Lamont-Doherty Earth Observatory, Columbia University, USA

[3]Institute of Earth Sciences, University of Iceland, Iceland

[4]CNRS/UMR 5563, Université Paul Sabatier, France

[5]Earth Science, University College London, UK

[6]Reykjavik Energy, Iceland

[7]European Commission, Joint Research Center, Institute for Energy and Transport, Petten, The Netherlands

[8]Iceland GeoSurvey, Reykjavik, Iceland

[9]Department of Applied Geology, Curtin University, Perth, Western Australia

[10]Nano-Science Center, Department of Chemistry, University of Copenhagen, Denmark

Carbon capture and storage (CCS) provides a solution towards decarbonization of the global economy. The success of this solution depends on the ability to safely and

permanently store CO_2. This study demonstrates for the first time the permanent disposal of CO_2 as environmentally benign carbonate minerals in basaltic rocks. We find that over 95% of the CO_2 injected into the CarbFix site in Iceland was mineralized to carbonate minerals in less than two years. This result contrasts with the common view that the immobilization of CO_2 as carbonate minerals within geologic reservoirs takes several hundreds to thousands of years. Our results, therefore, demonstrate that the safe long-term storage of anthropogenic CO_2 emissions through mineralization can be far faster than previously postulated.

The success of geologic CO_2 storage depends on its long-term security and public acceptance in addition to regulatory, policy, and economical factors (*1*). CO_2 and brine leakage through a confining system above the storage reservoir or through abandoned wells is considered as one of the major challenges associated with geologic CO_2 storage [e.g. (*2, 3, 4*)]. Leakage rates into the atmosphere of ≤0.1% are required to ensure effective climate change mitigation [e.g. (*5, 6*)]. To avoid CO_2 leakage, caprock integrity needs to be evaluated and monitored (*7*). Leakage risk is further enhanced by induced seismicity, which may open fluid flow pathways in the caprock (*8*). Mineral carbonatization (i.e. the conversion of CO_2 to carbonate minerals) via CO_2-fluid-rock reactions in the reservoir minimizes the risk of leakage and thus facilitates long-term and safe carbon storage and public acceptance (*9*). The potential for carbonatization is, however, limited in conventional CO_2 storage reservoirs such as deep saline aquifers, and depleted oil and gas reservoirs in sedimentary basins due to the lack of calcium,

45 magnesium and iron rich silicate minerals required to form carbonate minerals (*10, 11*).
46 An alternative is to inject CO_2 into basaltic rocks, which contain up to 25% by weight of
47 calcium, magnesium and iron. Basaltic rocks are highly reactive, and one of the most
48 common rock types on Earth, covering ~10% of continental surface area and most of the
49 ocean floor [e.g. (*12, 13*)].
50
51 The CarbFix pilot project was designed to promote and verify *in situ* CO_2 mineralization
52 in basaltic rocks for the permanent disposal of anthropogenic CO_2 emissions (*14*). Two
53 injection tests were performed at the CarbFix injection site near the Hellisheidi
54 geothermal power plant: Phase I: 175 tons of pure CO_2 from January to March 2012, and
55 Phase II: 73 tons of a CO_2-H_2S gas mixture in June to August 2012, of which 55 tons were
56 CO_2. Note that H_2S is not only a major constituent of geothermal gases but also of CO_2-
57 rich sour gas. Since the cost of CCS is dominated by capture and gas separation, the
58 overall cost could be lowered substantially by injecting gas mixtures rather than pure
59 CO_2 (*9*). Hence, the purpose of the mixed CO_2 / H_2S injection was to assess the feasibility
60 of injecting impurities in the CO_2 stream.
61
62 The CarbFix injection site is situated about 25 km east of Reykjavik and equipped with a
63 2000 m deep injection well (HN02) and 8 monitoring wells ranging in depth from 150 to
64 1300 m (Fig. 1). The target CO_2 storage formation is between 400 and 800 m depth and
65 consists of basaltic lavas and hyaloclastites with lateral and vertical intrinsic
66 permeabilities of 300 and 1700 x 10^{-15} m^2, respectively (*15, 16*). It is overlain by low

permeability hyaloclastites. The formation water temperature and pH in the injection interval range from 20 to 33°C and from 8.4 to 9.4, and it is oxygen depleted (15). Due to the shallow depth of the target storage reservoir and the risk of CO_2 gas leakage through fractures, a novel CO_2 injection system was designed and used, which dissolves the gases into down-flowing water in the well during its injection (*17*). To avoid potential degassing, CO_2 concentration in the injected fluids was kept below its solubility at reservoir conditions (17). Once dissolved in water, CO_2 is no longer buoyant (17) and it immediately starts to react with the Ca-Mg-Fe-rich reservoir rocks.

Since dissolved or mineralized CO_2 cannot be detected by conventional monitoring methods such as seismic imaging, the fate of the injected CO_2 was monitored using a suite of chemical and isotopic tracers. The injected CO_2 was spiked with carbon-14 (^{14}C), to monitor its transport and reactivity (*18*). For the pure CO_2 and the CO_2 / H_2S injections, the ^{14}C concentrations of the injected fluids were 40.0 Bq/L ($^{14}C/^{12}C$: 2.16 x 10^{-11}) and 6 Bq/L ($^{14}C/^{12}C$: 6.5 x 10^{-12}), respectively. By comparison, the ^{14}C concentration in the reservoir prior to the injections was 0.0006 Bq/L ($^{14}C/^{12}C$: 1.68 x 10^{-13}). This novel carbon tracking method was previously proposed for geologic CO_2 storage monitoring but its feasibility has not been tested previously (*19, 20*). As $^{14}CO_2$ behaves chemically and physically identical as $^{12}CO_2$ and is only minimally affected by isotope fraction during phase transitions (*21*) it provides the means to accurately inventory the fate of the injected carbon.

89 In addition to ^{14}C, we continuously co-injected non-reactive but volatile sulfur
90 hexafluoride (SF_6) and trifluoromethyl sulfur pentafluoride (SF_5CF_3) tracers to assess
91 plume migration in the reservoir. The SF_6 was used during Phase I and SF_5CF_3 during
92 Phase II. The SF_6 and SF_5CF_3 concentrations in the injected fluids were 2.33×10^{-8}
93 ccSTP/cc and 2.24×10^{-8} ccSTP/cc, respectively.
94
95 The CO_2 and CO_2/H_2S mixtures, together with the tracers were injected into the target
96 storage formation fully dissolved in water pumped from a nearby well. Typical injection
97 rates during Phase I injection were 70 g/s for CO_2 and 1800 g/s for H_2O, respectively
98 (*17*). Injection rates during Phase II varied between 10 and 50 g/s for CO_2 and 417 and
99 2082 g/s for H_2O. The dissolved carbon concentration (DIC) and pH of the injectates
100 were 0.82 mol/L and 3.85 (at 20°C) for Phase I and 0.43 mol/L and 4.03 for Phase II. Fluid
101 samples for SF_6, SF_5CF_3, ^{14}C, DIC and pH analyses were collected without degassing using
102 a specially designed downhole sampler from the injection well HN02 (*22*) or with a
103 submersible pump from the first monitoring well HN04 located ca. 70 m downstream
104 from HN02 at 400 m depth below surface prior, during and post-injection (Tables S1 -
105 S3).
106
107 The arrival of the injectate from Phase I at the monitoring well HN04 was confirmed by
108 an increase in SF_6 concentration, and a sharp decrease in pH and DIC concentration (Fig.
109 2 A and B, Table S3). Based on the SF_6 data, the initial breakthrough in HN04 occurred
110 56 days after injection. Subsequently, the SF_6 concentration slightly decreased before a

111 further increase in concentration occurred, with peak concentration 406 days after
112 initiation of the injection. SF_5CF_3 behaves similarly (Fig. 2 A); its initial arrival was
113 detected 58 days after initiation of the Phase II injection, followed by decreasing
114 concentrations until 350 days after the injection started. Subsequently, the SF_5CF_3
115 concentration increased, consistent with the SF_6 tracer breakthrough curve. The double
116 peaks in these tracer breakthrough curves are also in agreement with results from
117 previous tracer tests showing that the storage formation consists of relatively
118 homogenous porous media intersected by a low volume and fast flow path that
119 channels about 3% of the tracer flow between HN02 and HN04 (*23*).
120
121 The time series of DIC, pH, and ^{14}C in HN04 are initially coincident with the SF_6 record,
122 showing peak concentrations in ^{14}C and DIC and a decrease in pH around 56 days after
123 injection (Figs. 2 B and 3). The small drop in pH and increase in DIC around 200 days
124 after injection is caused by the Phase II injection as confirmed by the SF_5CF_3 time series
125 (Fig. 2 A). The similar initial pattern in the tracer breakthrough curves and the DIC
126 concentration suggests identical transport behavior of carbon and tracers in the
127 reservoir. However, ^{14}C and DIC concentrations subsequently decreased and stayed
128 more or less constant for the remaining monitoring period, with the exception of a small
129 increase in concentration induced by the Phase II injection (Figs. 2 B and 3 A and B).
130
131 The fate of the injected CO_2 was quantified using mass balance calculations (*18*).

132 The resulting calculated DIC and ^{14}C concentrations are much higher than that measured
133 in the collected water samples, suggesting a loss of DIC and ^{14}C along the subsurface
134 flow path towards the monitoring well (Fig. 3 A and B). The most plausible mechanism
135 for this difference is carbonate precipitation. The differences between calculated and
136 measured DIC and ^{14}C indicate that >95% of the injected CO_2 was mineralized through
137 water-CO_2-basalt reactions between the injection (HN02) and monitoring (HN04) wells
138 within two years (Fig. 3 A and B). The initial peak concentrations in DIC and ^{14}C detected
139 around 56 days after injection suggest that travel time along the low volume fast
140 flowing flow path was too short for significant CO_2 mineralization to occur. Most of the
141 injected CO_2 was likely mineralized within the porous matrix of the basalt that allows for
142 longer fluid residence times and thus extended reaction time. This conclusion is
143 confirmed by 1) calculated fluid saturation states showing that the collected monitoring
144 fluids are at saturation or supersaturation with respect to calcite at all times except
145 during the initial low volume flow path contribution, 2) XRD and SEM-EDXS analysis of
146 secondary mineral precipitates collected from the submersible pump in monitoring well
147 HN04 after it was hauled to the surface, showing these precipitates to be calcite (*18*)
148 (figs. S1 – S3), and 3) the similarity in the ^{14}C concentration of the injected CO_2 and the
149 precipitated collected calcite (7.48±0.8 and 7.82±0.05 fraction modern).
150
151 Although monitoring continues, the time scale of the tracer and DIC data discussed is
152 limited to 550 days since most of the injected CO_2 was mineralized by this time (Figs. 2
153 and 3). This 550-day limit also coincides with the breakdown of the submersible pump in

154 HN04 monitoring well, which resulted in a 3-month gap in the subsequent monitoring
155 data. The pump was clogged and coated with calcite (*18*).
156
157 The fast conversion rate of dissolved CO_2 to calcite minerals in the CarbFix storage
158 reservoir is most likely the result of several key processes: 1) The novel CO_2 injection
159 system that injected water-dissolved CO_2 into the subsurface; 2) The relatively rapid
160 dissolution rate of basalt, releasing Ca, Mg and Fe ions required for the CO_2
161 mineralization; (3) The mixing of injected water with alkaline formation waters; and (4)
162 The dissolution of pre-existing secondary carbonates at the onset of the CO_2 injection,
163 which may have contributed to the neutralization of the injected CO_2-rich water via the
164 reaction
165 $CaCO_3 + CO_2 + H_2O = Ca^{2+} + 2HCO_3^-$.
166 Dissolution of pre-existing calcite is supported by the $^{14}C/^{12}C$ ratio of the collected fluid
167 samples, which suggest a 50% dilution of the carbon in the fluid, most likely via calcite
168 dissolution just after it arrives in the basaltic reservoir. Nevertheless, the mass balance
169 calculations clearly demonstrate that these pre-existing carbonates re-precipitated
170 during the mineralization of the injected CO_2.
171
172 The results of this study demonstrate that the nearly complete *in-situ* CO_2
173 mineralization in basaltic rocks can occur in less than 2 years. Once stored within
174 carbonate minerals leakage risk is eliminated and any monitoring program of the
175 storage site can significantly be reduced thus enhancing storage security and potentially

public acceptance. Note that natural aqueous fluids in basalts and those at the CarbFix site tend to be at or close to equilibrium with respect to calcite, limiting its redissolution (16). The upscaling of this basaltic carbon storage method requires substantial quantity of water and porous basaltic rocks (*9*). Both are widely available on the continental margins such as off the coast of the Pacific northwest of the United States (*12*).

References and Notes

1. B. Metz, O. Davidson, H. de Coninck, M. Loos, L. A. Meyer, Eds. *IPCC Special Report on Carbon Dioxide Capture and Storage* (Cambridge Univ. Press, New York, 2005).
2. A. Espisito, S. Benson, *SPE* **133603-MS** (2010).
3. B. Ellis et al., *Greenhouse Gases: Science and Technology* **1(3)**, 248-260 (2011).
4. J. M. Bielicki, M. F. Pollak, J. P. Fitts, C. A. Peters, E. J. Wilson, *Int. J. Greenh. Gas Control* **20**, 272-284 (2014).
5. P. M. Haugan, F. Joos, *Geophys. Res. Lett*. **31**, L18202 (2004).
6. B. Van der Zwaan, L. Smekens, *Environ. Model Assess.* **14**, 135-148 (2009).
7. H. S. Eggleston et al., Eds. IPCC guidelines for national greenhouse gas inventories – A primer (National Greenhouse Gas Inventories Programme, IGES, Japan, 2008).
8. M. D. Zoback, S. M. Gorelick, *PNAS* **109(26)**, 10164-10168 (2012).
9. S. R. Gislason, E. H. Oelkers, *Science* **344**, 373-344 (2014).
10. J. M. Matter, P.B. Kelemen, *Nature Geoscience* **2**, 837-841 (2009).
11. S. M. V. Gilfillan et al., *Nature* **458**, 614-618 (2009).

12. D. S. Goldberg, T. Takahashi, A. L. Slagle, *PNAS* **105(29)**, 9920-9925 (2008).

13. B. P. McGrail et al., *JGR* **111**, B12201 (2006).

14. S. R. Gislason et al., *Int. J. Greenhouse Gas Control* **4**, 537-545 (2010).

15. H. A. Alfredsson et al., *Int. J. Greenhouse Gas Control* **12**, 399-418 (2013).

16. E. S. Aradóttir et al., *Int. J. Greenhouse Gas Control* **9**, 24-40 (2012).

17. B. Sigfusson et al., *Int. J. Greenhouse Gas Control* **37**, 213-219 (2015).

18. Materials and methods are available as supplementary material on *Science* Online.

19. P.P. Bachelor et al., *J. Radioanal. Nucl. Chem.* **277(1)**, 85-89 (2008).

20. K. S. Lackner, S. Brennan, *Climatic Change* **96**, 357-378 (2009).

21. I. D. Clark, P. Fritz, *Environmental Isotopes in Hydrogeology* (Lewis Publisher, Boca Raton, New York, 1997).

22. H. A. Alfredsson, K. Mesfin, D. Wolff-Boenisch, *Greenhouse Gas Sci. Technol.* **5**, 1-11 (2015)

23. M. Rezvani Khalilabad, G. Axelsson, S. Gislason, *Mineral. Mag.* **72(1)**, 121-125 (2008).

24. M. Stuiver, H. A. Polach, *Radiocarbon* **19(3)**, 355-363 (1977).

25. D. L. Parkhurst, C. A. J. Appelo, Description of input and examples for PHREEQC version 3, U.S. Geological Survey Techniques and Methods, book 6, 497 pp. (2013).

26. W. Stumm, J. J. Morgan, Aquatic Chemistry: Chemical equilibria and rates in natural waters (third ed.), John Wiley & Sons, New York, 1022 pp. (1996).

27. N. Assayag, J. Matter, M. Ader, D. Goldberg, P. Agrinier, *Chem. Geol.* **265**, 227-235 (2009).

28. D. L. Graf, *American Mineralogist* **46**, 1283 (1961).

29. S. A. Markgraf, R. J. Reeder, *American Mineralogist* **70**, 590 (1985).

30. H. T. Schaef, B. P. McGrail, *Appl. Geochem.* ***24****, 980-987 (2009)*

31. D. Wolff-Boenisch, S. Wenau, S. R. Gislason, E. H. Oelkers *Geochem. Cosmochim. Acta* **75**, 5510-5525 (2011).

32. A. P. Gysi, A. Stefansson, *Geochem. Cosmochim. Acta* **81**, 129-152 (2012).

33. I. Galeczka, D. Wolff-Boenisch, E. H. Oelkers, S. R. Gislason, *Geochem. Cosmochim. Acta* **126**, 123-145 (2014).

34. P. Cubillas et al. *Geochem. Cosmochim. Acta* **69**, 5459 (2005).

Acknowledgments: We acknowledge funding from Reykjavik Energy, U.S. Department of Energy under Award Number DE-FE0004847 to J.M.M and M.S., the European Commission through the projects CarbFix (EC coordinated action 283148), Min-GRO (MC-RTN-35488), Delta-Min (PITN-GA-2008-215360) and CO_2-REACT (EC Project 317235) to S.R.G., E.H.O. and Reykjavik Energy, and Nordic fund 11029-NORDICCS, the Icelandic GEORG Geothermal Research fund (09-02-001) to S.R.G and Reykjavik Energy. We thank Trausti Kristinsson and Einar Örn Þrastarsonfor for helping with sample collection in the field. All data used in this study are included in the supplementary material.

Figures

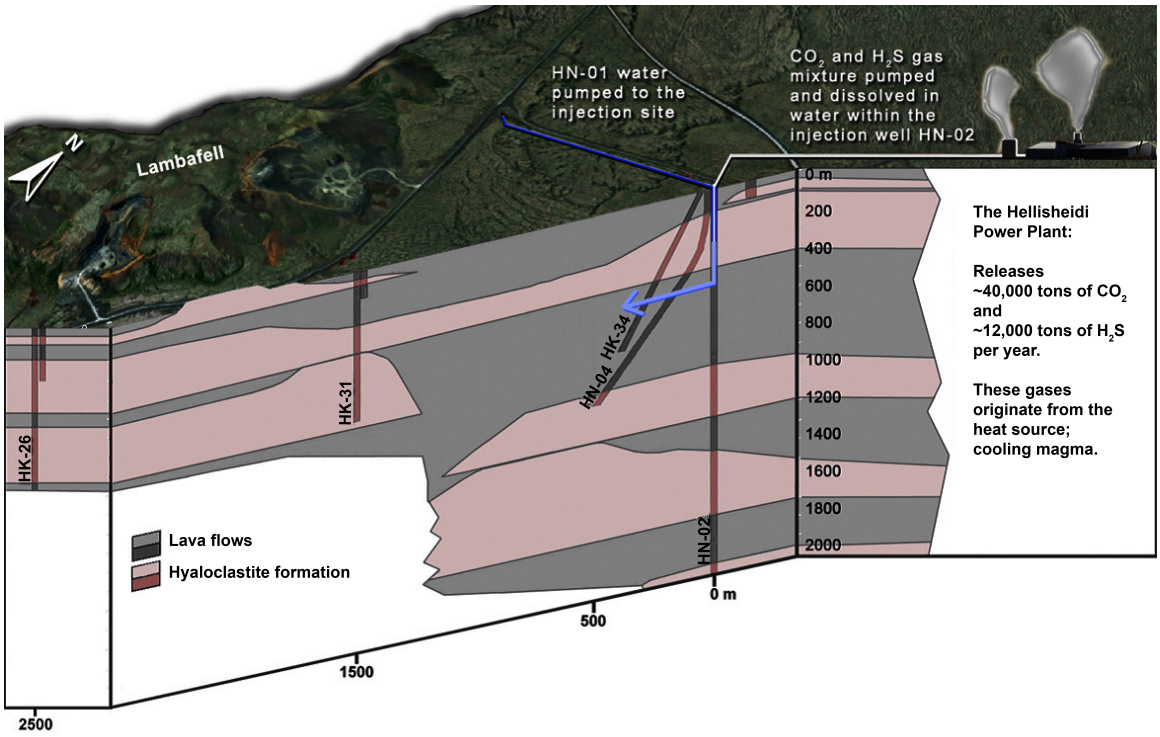

Fig. 1. Geological cross-section of the CarbFix injection site. CO_2 and H_2S are injected fully dissolved in water in injection well HN02 at a depth between 400 and 540 m. Fluid samples for this study, where collected in HN02 and the monitoring well HN04 (modified from *15*).

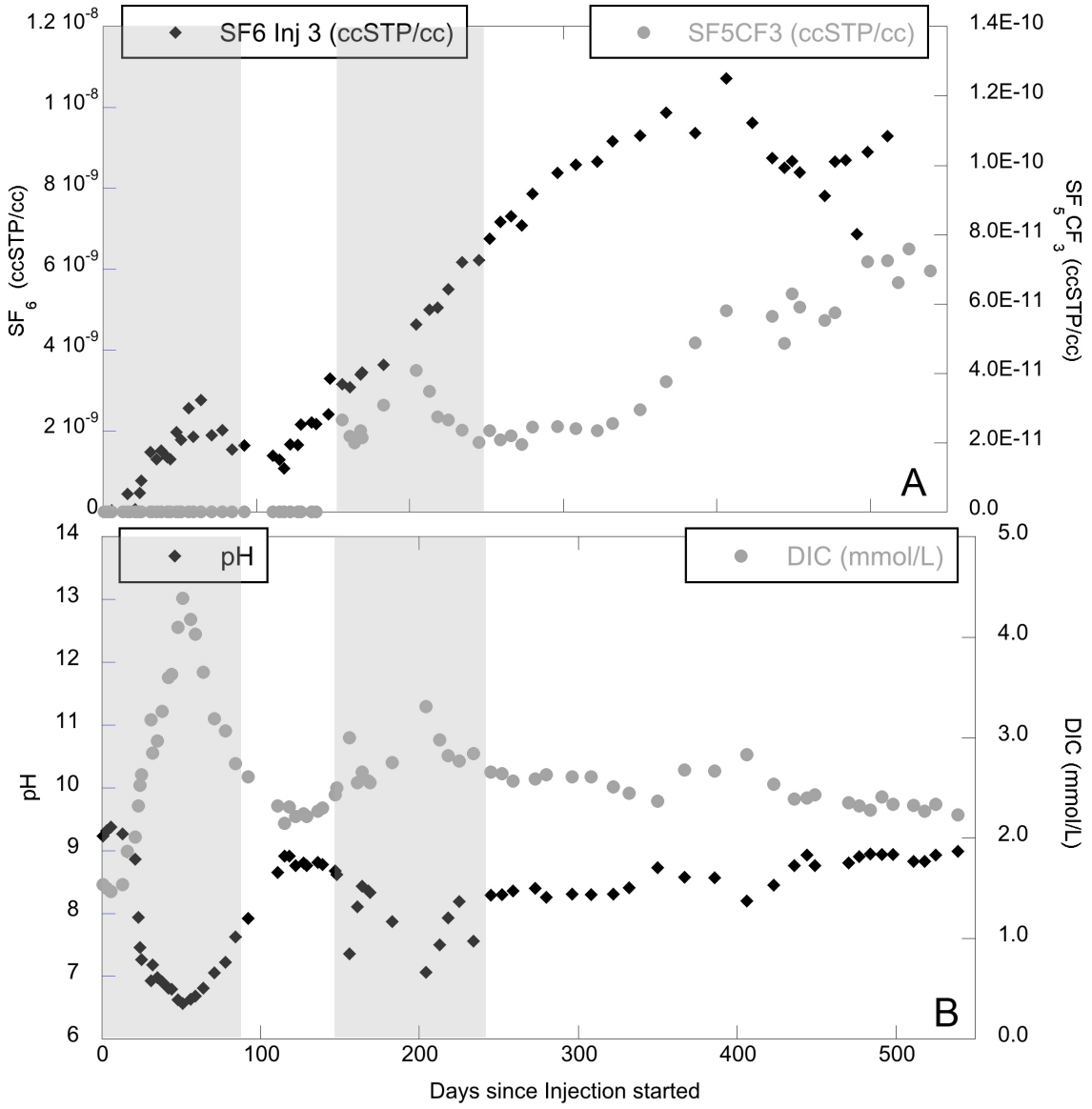

Fig. 2. Time series of (**A**) SF_6 and SF_5CF_3 tracer concentrations (ccSTP/cc), and (**B**) pH and dissolved inorganic carbon (DIC) in monitoring well HN04 for the pure CO_2 and the CO_2 & H_2S injections. Shaded area indicates Phase I and II injection period.

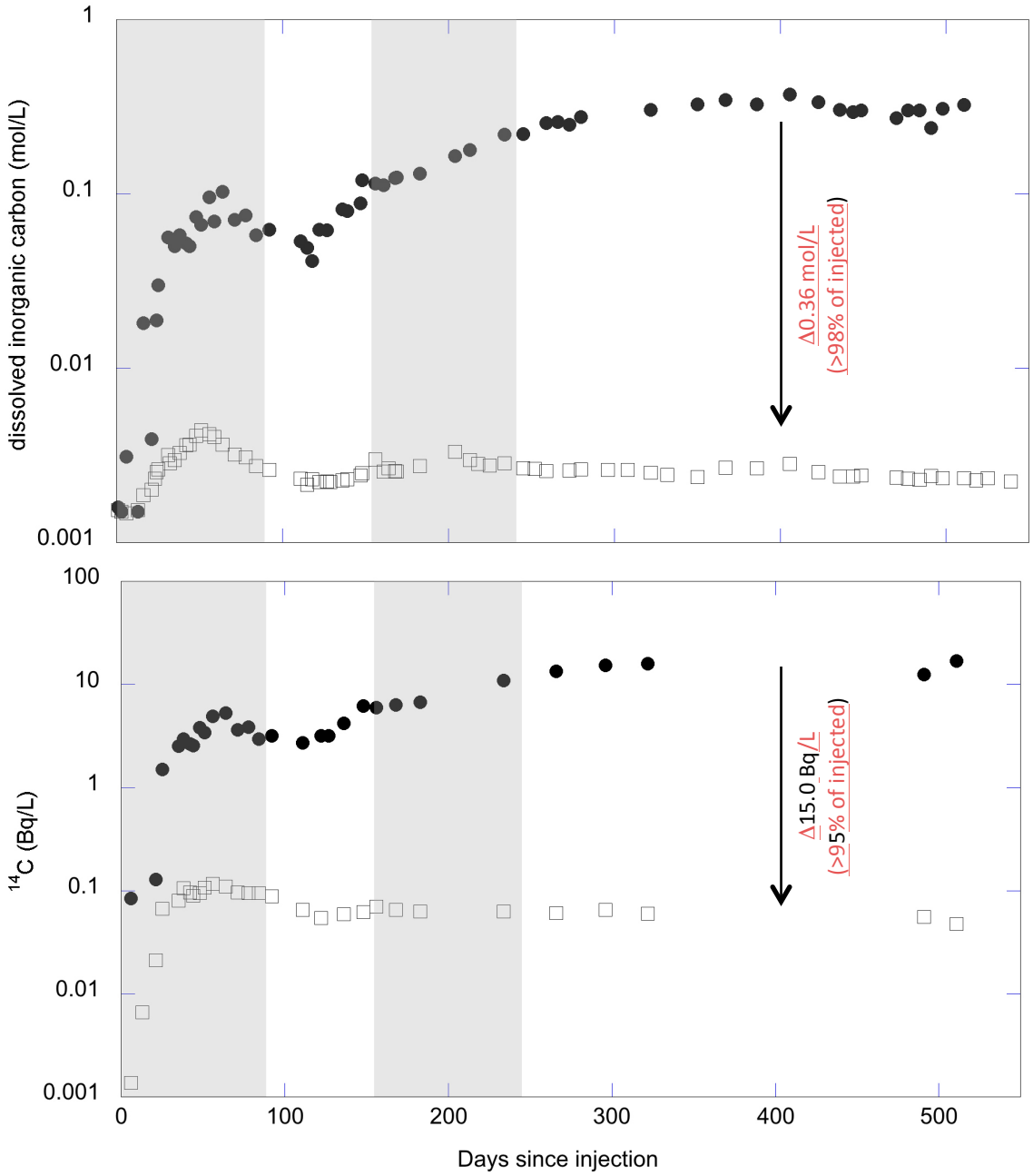

Fig. 3. (**A**) Time series of expected (full circles) vs. measured (empty squares) dissolved inorganic carbon (DIC, mol/L) in monitoring well HN04, indicating >98% conversion of injected CO_2 to carbonate minerals, and (**B**) time series of expected (full circles) vs. measured (empty squares) $^{14}C_{DIC}$ (Bq/L) in monitoring well HN04, showing >95% of injected CO_2 to be converted to carbonate minerals. Shaded area indicates Phase I and II injection period.

Supplementary Materials for

Rapid carbon mineralization for permanent disposal of anthropogenic carbon dioxide emissions

Matter et al.

Materials and Methods

1) The SF_6 and SF_5CF_3 tracers

SF_6 and SF_5CF_3, originally stored in gas cylinders, were mixed into the CO_2 and CO_2+H_2S flue gas stream using mass flow controllers. Carbon-14 was added to the water injection stream as an aqueous $H^{14}CO_3^-$ solution using a Milton Roy micro-dosing pump (Model AA973-352S3). The $H^{14}CO_3^-$ solution was created by adding 10 mCi of a ^{14}C-rich sodium bicarbonate aqueous solution obtained from Perkin Elmer to 100 liter of groundwater collected from the target storage reservoir prior to CO_2 injection.

Fluid samples for SF_6 and SF_5CF_3 analyses were collected in evacuated 100 ml glass serum bottles from the monitoring well HN04. Concentrations in the headspace were measured with a precision of ±2% using gas chromatography (SRI 8610C) and ultrapure nitrogen as the carrier gas. The headspace samples were injected into a 6ft long, 1/8” wide pre-column with a 5 ångström molecular sieve (MS-5A) and a 6ft chromatographic column at 60°C. SF_6 and SF_5CF_3 concentrations were measured using a SRI 8610C gas chromatograph with an

electron capture detector and a Alltech Carbograph column. Results were recorded using the PeakSimple 3.07.2 software, and concentrations in the water samples were calculated based on the volume of headspace and the solubility.

The SF_6 concentration data from the Phase I injection had to be corrected for the SF_6 that originated from a previous hydrological tracer test. In 2008, we injected SF_6 and sodium fluorescein (Na-Flu) into the target storage reservoir during a short duration tracer test to characterize the hydrology of the injection site. During the Phase I CO_2 injection only SF_6 was injected. Thus, the difference between the observed Na-Flu and the SF_6/Na-Flu ratio can be used to calculate how much SF_6 in the collected water samples is from the Phase I injection (Table S2). Without the addition from the Phase I injection, the SF_6/Na-Flu ratio would follow the trajectory of the Na-Flu concentration. Thus, multiplying the expected ratio by the observed Na-Flu concentration provides a measure of the expected SF_6 concentration. The difference between the observed and expected SF_6 concentration is the actual SF_6 from the Phase I injection (Table S2).

2) Carbon-14

Fluid samples for ^{14}C analysis were collected in 125 ml glass serum bottles. For ^{14}C analysis, water samples were acidified to release the dissolved inorganic carbon as CO_2. The ^{14}C concentration was measured with ^{14}C-AMS first in the W.M. Keck Carbon Cycle Accelerator Mass Spectrometry Laboratory at the University of California, Irvine, and later in the BioAMS laboratory at Lawrence Livermore National Laboratory, USA. Results are reported as fractions of the Modern Standard, $\Delta^{14}C$, following the conventions of Stuiver and Polach (*24*). All results are corrected for isotopic fractionation with $\delta^{13}C$ values measured on prepared samples using AMS spectrometer. Data and uncertainties are reported in Table S2.

3) Dissolved inorganic carbon (DIC)

Dissolved inorganic carbon (DIC) was calculated using PHREEQC (*25*) from measured pH, alkalinity, *in-situ* temperature and total dissolved element concentration measurements. The pH was determined in the field with a Eutech InstrumentsTM CyberScan pH 110 electrode calibrated using NBS standards, and verified in the laboratory a few hours after sampling with a Cole Parmer glass pH electrode. Alkalinity titration was performed using the Gran function to determine the end point of the titration (*26*). The concentration of major elements including Si, Ca, K, Mg, Na, and S and the trace metals Fe and Al were determined by Inductively Coupled Plasma Optical Emission Spectrometry (ICP-OES) using an in-house multi-elements standard checked against the SPEX Certified Reference standard at the University of Iceland. The uncertainties on calculated DIC measurements are estimated to be ±5%

4) Mass balance calculations

Mass balance calculations for dissolved inorganic carbon and ^{14}C were performed to assess the reactivity of the injected CO_2 (27). The mixing fraction between the injected solution (IS) and ambient groundwater (BW) was calculated for each extracted water sample (i) using

$$\left[SF_6\right]_i = X\left[SF_6\right]_{IS} + \left(1-X\right)\left[SF_6\right]_{BW} \quad (1)$$

with *X* being the fraction of injected solution in the extracted water sample. The expected DIC and ^{14}C values due to pure mixing was then determined from

$$DIC_{mix} = X \cdot DIC_{IS} + (1-X) \cdot DIC_{BW} \quad (2)$$

and

$$^{14}C_{mix} = X \cdot {}^{14}C_{IS} + \left(1-X\right) \cdot {}^{14}C_{BW} \quad (3)$$

Differences in DIC and ^{14}C concentrations between the values measured in the retrieved fluid samples and the expected values assuming only mixing between injectate and ambient groundwater yield the loss of DIC and ^{14}C due to carbonate precipitation.

5) Analysis of solid phases

Mineral precipitate samples collected from the submersible pump in monitoring borehole HN04 were analyzed by X-Ray diffraction (XRD), scanning electron microscopy (SEM), and energy dispersive X-ray spectroscopy (EDXS) mapping. Prior to analysis, the samples were stored and treated in an anaerobic chamber to minimize oxidation.

Samples for XRD were mounted on low background Si sample holders and covered with an X-ray transparent cup (Bruker) to decrease oxidation of the fine-grained material during measurement. Measurements were conducted on a Bruker D8 DISCOVER equipped with a LynxEye detector and a Co-source. Scan range was 5-80° using a 0.05° step size and a count time of 10 s per step. Two types of samples were prepared for SEM-EDXS. One set was mounted directly on the Al-sample stubs to avoid a carbon signal from carbon tape. The material was resuspended in anoxic ethanol and a drop of it transferred to the sample holder and left to dry. These samples were imaged by SEM using low vacuum (60 Pa) to minimize sample charging. For another set of samples, the Al-sample holders were covered with carbon tape and grains were picked from the samples and mounted upright to enable imaging of these grains perpendicular to the growth direction. These samples were sputter coated with Au and imaged under high vacuum (4×10^{-4} Pa) to resolved detailed morphological features. SEM/EDXS measurements were conducted on a FEI Quanta 3D FEG SEM equipped with an Oxford instrument X-max 20 mm^2 EDXS detector having a nominal energy resolution of 0.125 keV for Mn$K\alpha$ (FWMH). During imaging, accelerating voltage was 20 KeV and currents were 3.8 pA for SEM imaging and 8 nA for EDXS mapping. In the EDXS maps, color intensity for an element is linearly correlated with the integrated intensity measured in a narrow range round it characteristic X-ray (Ca$K\alpha$: 3.63-3.75 KeV; Fe$K\alpha$: 6.32-6.48 KeV; Si$K\alpha$: 1.69-1.79 KeV; O$K\alpha$: 0.49-0.56 KeV; C$K\alpha$: 0.24-0.29 KeV; peak from C$K\alpha$ has a slight contribution of <5% from Au_N lines).

XRD of all materials from the monitoring borehole (Fig. S1) shows only the Bragg peaks expected for calcite [e.g. (*28, 29*)]. Please note that the broad peaks between 10 and 30° are from the cap protecting the sample from oxidation. SEM imaging and EDXS mapping clearly show 10 um to 1 mm slightly elongated grains rich in Ca, C, and O, as expected for calcite, with trace concentrations of Mg, Mn, and Fe (Fig. S2). Imaging of samples EDXS mapping of the grains collected from inside the pump shows a banded structure where they were fractured, with a first generation of calcite containing rich in Fe- and Si and a second generation largely without such material (Fig. S3).

Laboratory studies of basalt carbonation.

A large number of laboratory experiments have been performed to assess the feasibility of basalt carbonation as a carbon storage strategy (e.g. 15, 16, 30, 31, 32, 33). Such experiments demonstrate the efficient carbonation of basalts and its constituent minerals. During basalt-water-CO_2 interaction, calcium liberated by basalt dissolution tends to provoke calcite precipitation, whereas the liberated magnesium, aluminum and silicon tend to provoke the formation of zeolite and clay minerals (15, 16, 32).

Several experimental studies have been aimed at assessing if precipitated carbonate minerals would eventually slow the overall carbonation rates of basalts and its constituent minerals (9,10). Such studies suggest that the carbonate minerals that precipitate on the surfaces of these rocks and minerals have little effect on the dissolution rates of the original solid and on their carbonation rates. These results were attributed to the poor structural match between the dissolving silicate and precipitating carbonate, which leaves sufficient pathways for chemical mass transfer to and from the adjoining fluid phase (e.g. 34). Such results suggest that the in-situ carbonation of basalts will be little effected by the precipitation of carbonate phases on their surfaces.

In situ fluid chemistry and transport

Representative pre-injection fluid chemistries at the injection site are summarized in Table S2. The temperature gradient at the injection site is 80 °C/km. Groundwater flow in the top tens of meters is to southwest (16); water flow in the lower part of the system is focused in lava flows located at the CO_2 injection depth of 400–800 m depth. The flow rate in this lower system is on the order of 25 m per year and the hydraulic head decreases toward southwest (15, 16). Hydrological models, pump tests and tracer tests, suggest that the effective matrix porosity of this lava formation is 8.5% (16).

The injection of CO_2-charged waters lead to a pH drop in the formation waters provoking the dissolution of basalt and the eventual precipitation of carbonate minerals. In addition to the natural ambient water flow in the target basaltic reservoir, advective transport in the system was enhanced by the continuous pumping of water into the HN-02 injection well and pumping of water from the HN-04 monitoring well at a rate of 1 l/s throughout the study period. The dominance of advection as the chemical transport mechanism in the system is evident in the concentration of chemical tracer in the monitoring fluid shown in Fig. 2; aqueous diffusion is far too slow to transport substantial material from the injection to the monitoring well over the 2-year study period.

Supporting Tables

Table S1. Injection test parameters, including results from the tracer and chemical analysis of injectate.

Injection Phase	CO_2 (tons)	H_2O (liters)	SF_6 (ccSTP/cc)	SF_5CF_3 (ccSTP/cc)	^{14}C (fraction modern)	DIC (mol/L)	pH
I	175	4.8×10^{6}	2.33×10^{-8}	none	16.17	0.82	3.85 (@20°C)
II	54.75	2.25×10^{6}	none	2.24×10^{-8}	4.65	0.43	4.03 (@20°C)

Table S2. Representative water chemistries at the CarbFix injection site prior to the gas injections (after 15).

	Well		
Parameter or aqueous concentration	HN-1 (source of injection water)	HN-2	HN-4
Sample	08HAA02	09HAA16	08HAA01
Sampling date	1 July 2008	19 May 2009	1 July 2008
Temperature °C	19.0	15.5	32.3
pH at 20 ±2 °C	8.87	8.79	9.43
O_2 (mmol/L)	0.057	0.011	0.037
Alkalinity (meq/kg)	1.91	1.45	1.91
F (mmol/L)	0.014	0.013	0.026
Cl (mm/L)	0.247	0.222	0.228
SO_4 (mmol/L)	0.075	0.077	0.089
Na (mmol/L)	1.301	1.338	2.114
K (mmol/L)	0.027	0.012	0.019
Ca (mmol/L)	0.164	0.124	0.041
Mg (mmol/L)	0.313	0.149	0.005
Fe (µmol/)	0.016	0.399	0.064
Al (µmol/)	0.419	0.097	1.905
Si (mmol/L)	0.363	0.337	0.897

Table S3: Result from the tracer and chemical fluid analyses.

Sample ID	Days since injection started	Na-Flu (g/L)	SF_6 (ccSTP/cc)	SF_6 Phase I (ccSTP/cc)*	SF_5CF_3 Phase II (ccSTP/cc)	pH	DIC (mmol/ L)	^{14}C (frac. modern)	±	^{14}C (Bq/L)
619	1	4.94E-05	1.51E-09	2.44E-12		9.24	1.54			
621	2		1.54E-09							
623	3	4.98E-05	1.45E-09			9.32	1.5			
629	6	5.05E-05	1.62E-09	4.34E-11		9.38	1.47	0.3119	0.0008	0.001377
643	13	5.15E-05	1.56E-09			9.27	1.54	1.328	0.002	0.006584
651	16	5.15E-05	2.09E-09	4.52E-10		8.98	1.87			
655	18		1.90E-09							
661	21	5.14E-05	1.70E-09	6.58E-11		8.86	2.01	3.5054	0.0049	0.02117
665	23		2.02E-09			7.94	2.32			
667	24	5.14E-05	2.10E-09	4.70E-10		7.46	2.53			
669	25	5.14E-05	2.41E-09	7.75E-10		7.27	2.63	8.4908	0.0119	0.06685
679	31	5.23E-05	3.18E-09	1.48E-09		6.93	3.18			
681	32		3.25E-09			7.18	2.85			
687	35	5.36E-05	3.09E-09	1.31E-09		6.98	2.97	9.0563	0.0217	0.08001
693	38	5.43E-05	3.35E-09	1.52E-09		6.91	3.26	10.8941	0.0516	0.10575
699	42	5.54E-05	3.26E-09	1.36E-09		6.81	3.6	9.8633	0.0338	0.09663
703	44	5.46E-05	3.16E-09	1.31E-09		6.79	3.63	9.2766	0.0647	0.08921
705	48	5.00E-05	3.52E-09	1.97E-09		6.63	4.1	9.1683	0.0641	0.09506
709	49		3.70E-09							
715	51	4.92E-05	3.27E-09	1.78E-09		6.57	4.39	9.908	0.0758	0.10749
721	56	4.90E-05	4.05E-09	2.57E-09		6.64	4.18	10.9666	0.0696	0.11732
723	59	4.90E-05	3.34E-09	1.86E-09		6.68	4.03			
733	64	4.88E-05	4.24E-09	2.78E-09		6.81	3.65	11.1269	0.0637	0.10968
741	71	4.86E-05	3.36E-09	1.91E-09		7.06	3.19	10.3135	0.0805	0.09608
747	78	4.85E-05	3.47E-09	2.03E-09		7.22	3.07	10.963	0.089	0.09488
753	84	4.83E-05	2.99E-09	1.55E-09		7.63	2.74	10.963	0.089	0.09488
763	92	5.03E-05	3.21E-09	1.65E-09		7.92	2.61	11.2236	0.1119	0.08778
775	111	5.51E-05	3.28E-09	1.40E-09		8.65	2.32	9.0533	0.052	0.06502
777	115	4.96E-05	2.81E-09	1.30E-09		8.92	2.15			
781	118	4.90E-05	2.56E-09	1.08E-09		8.92	2.31			
783	122	4.85E-05	3.12E-09	1.67E-09		8.76	2.22	8.0588	0.0616	0.05473
785	127	4.74E-05	3.04E-09	1.66E-09		8.81	2.24			
787	129	4.70E-05	3.52E-09	2.16E-09		8.76	2.22			
789	136	4.57E-05	3.49E-09	2.21E-09		8.82	2.27	8.6288	0.0795	0.05938
793	139	4.50E-05	3.41E-09	2.17E-09		8.78	2.3			
797	147	4.29E-05	3.53E-09	2.41E-09		8.68	2.43			
801	148	4.29E-05	4.42E-09	3.30E-09		8.62	2.5	8.4219	0.0742	0.06251
803	149		4.04E-09							
813	156	4.16E-05	4.22E-09	3.17E-09	2.66E-11	7.36	3	8.0027	0.0593	0.06998

819	161	4.18E-05	4.15E-09	3.09E-09	2.18E-11	8.11	2.55			
825	164		4.19E-09		1.99E-11	8.43	2.66			
831	168	4.00E-05	4.37E-09	3.40E-09	2.35E-11	8.36	2.57	8.4363	0.0521	0.06516
833	169	3.90E-05	4.37E-09	3.45E-09	2.14E-11	8.33	2.55			
841	183	3.78E-05	4.50E-09	3.64E-09	3.09E-11	7.87	2.75	7.769	0.0512	0.0628
847	204	3.64E-05	5.43E-09	4.64E-09	4.09E-11	7.07	3.31			
849	213	3.60E-05	5.78E-09	5.01E-09	3.49E-11	7.50	2.98			
850	218	3.56E-05	5.81E-09	5.06E-09	2.75E-11	7.93	2.82			
851	225	3.51E-05	6.23E-09	5.50E-09	2.65E-11	8.19	2.77			
853	234	3.42E-05	6.87E-09	6.17E-09	2.36E-11	7.56	2.84	7.9298	0.0512	0.06267
855	245	3.37E-05	6.90E-09	6.22E-09	2.01E-11	8.29	2.66			
857	252	3.34E-05	7.42E-09	6.76E-09	2.35E-11	8.30	2.64			
858	259	3.34E-05	7.84E-09	7.18E-09	2.08E-11	8.36	2.57			
859	266	3.26E-05	7.94E-09	7.32E-09	2.20E-11			7.4848	0.0776	0.06051
860	273	3.21E-05	7.69E-09	7.08E-09	1.95E-11	8.40	2.59			
861	280	3.09E-05	8.42E-09	7.86E-09	2.45E-11	8.26	2.63			
863	296	3.00E-05	8.92E-09	8.39E-09	2.46E-11	8.31	2.61	8.4791	0.0742	0.06498
865	308	2.94E-05	9.09E-09	8.58E-09	2.42E-11	8.30	2.61			
869	322	2.92E-05	9.15E-09	8.66E-09	2.35E-11	8.31	2.51	8.3668	0.0657	0.06009
873	332	2.88E-05	9.65E-09	9.17E-09	2.56E-11	8.41	2.45			
875	350	2.88E-05	9.79E-09	9.31E-09	2.96E-11	8.73	2.37			
877	367	2.69E-05	1.03E-08	9.88E-09	3.77E-11	8.58	2.68			
879	386	2.47E-05	9.72E-09	9.37E-09	4.88E-11	8.57	2.67			
881	406	2.31E-05	1.10E-08	1.07E-08	5.81E-11	8.20	2.83			
883	423	2.33E-05	9.94E-09	9.63E-09	5.65E-11	8.45	2.54			
881	436	2.26E-05	9.03E-09	8.75E-09	4.87E-11	8.76	2.39			
889	444	2.15E-05	8.77E-09	8.52E-09	6.30E-11	8.93	2.4			
893	449	2.17E-05	8.93E-09	8.67E-09	5.92E-11	8.76	2.43			
895	454	2.15E-05	8.65E-09	8.40E-09	5.52E-11					
897	470	2.13E-05	8.07E-09	7.82E-09	5.76E-11	8.81	2.35			
901	477	2.09E-05	8.90E-09	8.66E-09		8.91	2.32			
905	484	2.05E-05	8.93E-09	8.70E-09		8.95	2.28			
907	491	1.92E-05	7.07E-09	6.87E-09		8.94	2.41	7.5505	0.0467	0.05559
909	498	1.92E-05	9.10E-09	8.91E-09		8.94	2.34			
913	511	2.20E-05	9.57E-09	9.30E-09	7.26E-11	8.83	2.33	6.5517	0.0472	0.04745
915	518		8.28E-09		6.61E-11	8.83	2.27	6.2029		0.04231
917	525		9.80E-09		7.59E-11	8.93	2.34	7.2165		0.05075
918	539		9.39E-09		6.96E-11	8.99	2.23	6.6135		0.04571

Supporting Figures

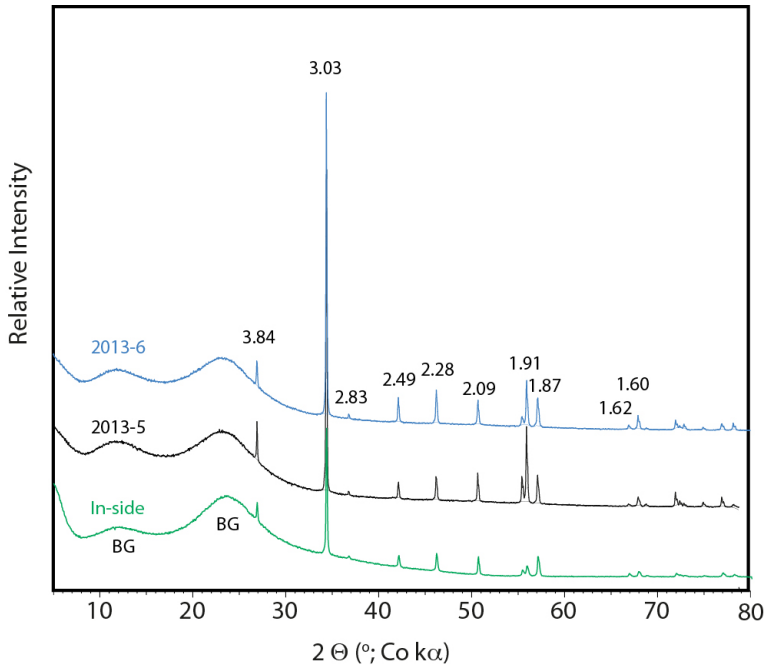

Figure S1. X-ray tracers of sample 2013-5 and 2013-6 taken from the submersible pump. The two broad peaks are from the cap protecting the sample from further oxidation is marked BG.

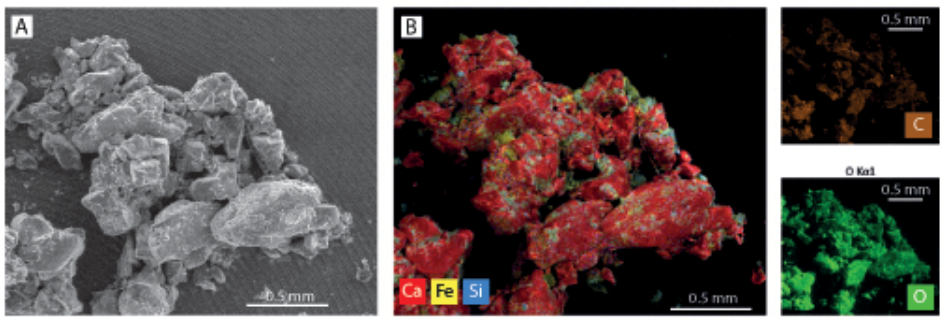

Figure S2. Overview SEM images and EDX maps of material from sample 2013-6. (**A**) SEM image. (**B**) EDX map of are shown in SEM image A. The maps for Ca, Fe and Si has been overlain the SEM image, whereas the maps for C and O are presented individually.

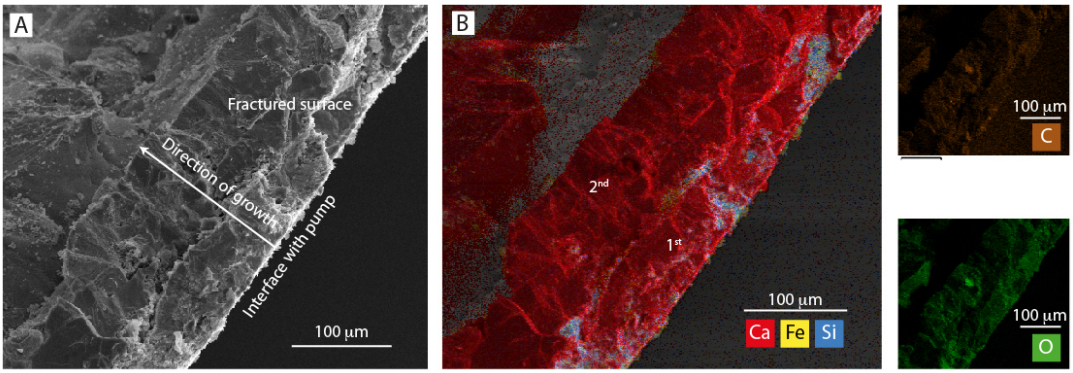

Figure S3. SEM images and EDX maps of fractured flake from a sample collected inside the submersible pump. (**A**) SEM image of the fractured flake mounted upright so that the internal regions of the material could be imaged. Fractured region, where the material interfaced with the pump surface and the direction of mineral growth is indicated. (**B**) EDX maps of area shown in SEM image A. The maps for Ca, Fe and Si has been overlain the SEM image, whereas the maps for C and O are presented individually. The location of two generations of calcite have been indicated based on the frequency of Fe- and Si-rich material.